Nanoscale quantification of intracellular element concentration by X-ray fluorescence microscopy combined with X-ray phase contrast nanotomography

Chiara Gramaccioni, Yang Yang, Alessandra Procopio, Alexandra Pacureanu, Sylvain Bohic, Emil Malucelli, Stefano Iotti, Giovanna Farruggia, Inna Bukreeva, Andrea Notargiacomo, Michela Fratini, Piera Valenti, Luigi Rosa, Francesca Berlutti, Peter Cloetens, and Stefano Lagomarsino

Citation: Appl. Phys. Lett. **112**, 053701 (2018); doi: 10.1063/1.5008834

View online: https://doi.org/10.1063/1.5008834

View Table of Contents: http://aip.scitation.org/toc/apl/112/5

Published by the American Institute of Physics

Nanoscale quantification of intracellular element concentration by X-ray fluorescence microscopy combined with X-ray phase contrast nanotomography

Chiara Gramaccioni,[1,2] Yang Yang,[3] Alessandra Procopio,[4] Alexandra Pacureanu,[3] Sylvain Bohic,[3,5] Emil Malucelli,[4] Stefano Iotti,[4] Giovanna Farruggia,[4] Inna Bukreeva,[2] Andrea Notargiacomo,[6] Michela Fratini,[2,7] Piera Valenti,[8] Luigi Rosa,[8] Francesca Berlutti,[8] Peter Cloetens,[3] and Stefano Lagomarsino[2]

[1]*Department of Physics, University of Calabria, Arcavata di Rende, 87036 Italy*
[2]*CNR-Nanotec, c/o Department of Physics University Sapienza, 00185 Roma, Italy*
[3]*European Synchrotron Radiation Facility, 38043 Grenoble, France*
[4]*Department of Pharmacy and biotechnology, University Bologna, 40127 Bologna, Italy*
[5]*INSERM U836, Grenoble Institute of Neuroscience, 38700 Grenoble, France*
[6]*Institute for Photonics and Nanotechnologies - CNR, 00156 Roma Italy*
[7]*Fondazione Santa Lucia, 00179 Roma, Italy*
[8]*Department of Public Health and Infectious Diseases, University Sapienza, 00185 Roma, Italy*

(Received 10 October 2017; accepted 13 December 2017; published online 30 January 2018)

We present here a correlative X-ray microscopy approach for quantitative single cell imaging of molar concentrations. By combining the elemental content provided by X-ray fluorescence microscopy and the morphology information extracted from X-ray phase nanotomography, we determine the intracellular molarity distributions. This correlative method was demonstrated on a freeze-dried human phagocytic cell to obtain the absolute elemental concentration maps of K, P, and Fe. The cell morphology results showed a very good agreement with atomic-force microscopy measurements. This work opens the way for non-destructive single cell chemical analysis down to the sub-cellular level using exclusively synchrotron radiation techniques. It will be of high interest in the case where it is difficult to access the morphology using atomic-force microscopy, for example, on frozen-hydrated cells or tissues. https://doi.org/10.1063/1.5008834

The question of intracellular element quantification is central in quantitative biology. It is important to know not only the total content of present elements, but also their spatial distribution. In this paper, we present a multimodal approach based exclusively on two synchrotron radiation techniques: hard X-ray Fluorescence Microscopy (XRFM) and propagation based phase contrast X-ray nanotomography (X-ray holotomography). XRFM provides the spatial distribution of different elements simultaneously and has been used to map trace elements in cells.[1–3] XRFM gives the total amount of selected atoms excited in each illuminated pixel. However, the most relevant measurement for biological studies is the concentration or the mass fraction. In this case, XRFM must be complemented with techniques that give information on the cell morphology (volume or thickness) or on the cell total mass. Several papers dealing with this issue have been published.[4–8] Lagomarsino *et al.*[6] and Malucelli *et al.*[7] used atomic-force microscopy (AFM), to obtain the sample morphology with nanometer spatial resolution. After adequate data analysis procedures, the combination of XRFM and AFM allows us to obtain the elemental molarity, which is the most common quantity used to describe the cell biochemical processes. Both magnesium[6] and major cell component (carbon, oxygen, and nitrogen)[7] molarity maps have been obtained. Alternatively, Kosior *et al.*[8] determined the spatial distribution of mass fractions by combining XRFM and 2D synchrotron radiation phase contrast imaging. The latter technique is orders of magnitudes more sensitive than absorption imaging in the hard X-ray energy range. It relies on the quantitative determination of the phase shift introduced by the object, which is, to a good approximation, proportional to the projection of the mass density. Normalization of the X-ray fluorescence elemental map with the retrieved phase map will therefore give access to the spatial distribution of the element mass fraction.[8] Different setups allow combining XRFM and phase sensitive techniques, such as differential phase contrast,[9] Zernike phase contrast,[10] ptychography,[11,12] or holography.[13] However, the measurements are rarely combined to obtain quantitative fluorescence data. X-ray fluorescence tomography can in principle provide the molarity directly,[14] but it is not often used because of long scanning times and radiation damage effects.

In this paper, XRFM was combined with X-ray phase nanotomography to map the molarity of several elements at nanoscale spatial resolution, in particular, iron (Fe), potassium (K), and phosphorus (P). The use of phase contrast imaging in three dimensions is essential to obtain volumetric information without assuming a constant and known cell density. The focus on iron here stems from a broader research project studying the Fe homeostasis in inflamed cells, in the presence or absence of lactoferrin, which is an iron-chelating glycoprotein of natural immunity.[15–17]

Human macrophage cells were cultured in RPMI 1640 medium (Euroclone, Italy) supplemented with 10% calf

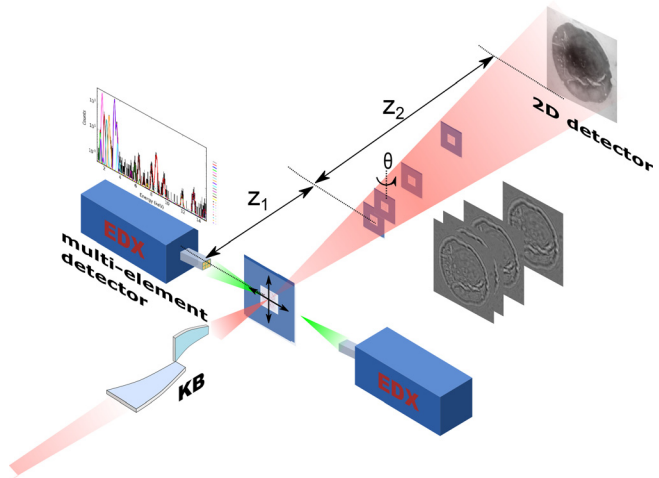

FIG. 1. Schematic of the experimental setup for combined X-ray fluorescence microscopy and phase nanotomography.

serum and grown on Si_3N_4 membranes held by $5 \times 5\,mm^2$ silicon frames. Freeze-dried samples were prepared to minimize the preparation artifacts for measurements at room temperature. This is accepted to be the most reliable room temperature specimen preparation method with a volume reduction of only 10%–15% and nearly no shrinkage between most of the cellular compartments.[18] The X-ray measurements were carried out at the Nano-Imaging beamline ID16A-NI at the European Synchrotron Radiation Facility (ESRF, Grenoble, France). This 185 m long beamline is equipped with a multilayer monochromator and a multilayer coated crossed Kirkpatrick-Baez mirror system, focusing the beam down to $25 \times 37\,nm^2$ (H×V). Two discrete energies, 17 keV and 33.6 keV, are offered by the beamline. The selected energy for our measurements was 17 keV, for better fluorescence excitation of the elements of biological interest. The samples were measured in high vacuum (10^{-7} mbar). This environment is compatible with cryogenic operation, avoids air scattering, and optimizes the detection of low Z elements.

XRFM measurements were carried out by continuous scanning of the sample through the focus with a pixel size of 100 nm and a dwell time of 50 ms. The X-ray fluorescence spectra were collected by a pair of 6-element silicon drift detectors (RaySpec Ltd., UK) positioned perpendicular to the incoming beam (see Fig. 1). For quantitative analysis, the fluorescence spectra were fitted using the open source PyMCA program.[19] The fundamental parameters of the experimental setup were calibrated with a thin film standard (AXO Dresden, GmbH). The areal density maps of phosphorus, potassium, and iron deduced from the fluorescence K-emission lines are shown in Fig. 2.

For X-ray phase nanotomography acquisition, the same sample was placed in the cone beam at a distance z_1 downstream of the focus. The 2D detector (a FReLoN charged-coupled device with binned 2048×2048 pixels array) was placed at a distance z_2 downstream of the sample, achieving a magnification $M = (z_1 + z_2)/z_1$ and an effective propagation distance $D = z_2/M$. The magnification was set to achieve a pixel size of 50 nm in the phase images. For better phase reconstruction,[20] acquisition has been made at four different focus-to-sample distances (specifically at 29, 30, 34, and 44 mm), as shown in Fig. 1. At each distance, a tomography scan was acquired consisting of 600 projections spanning half a turn. Due to the sample geometry (a Si_3N_4 membrane on a silicon frame), a range of angles was obscured leading to a missing wedge problem. The phase maps of the sample were retrieved via holographic reconstruction[20] based on the Fresnel diffraction patterns at different effective propagation distances. This allows overcoming the zero crossings in the frequency domain inherent in the contrast transfer functions. The retrieved phase maps are projections of the refractive index decrement, which is proportional to the electron density and to a good approximation the mass density. The projections were used for 3D tomographic reconstruction using the filtered back projection algorithm implemented in the ESRF PyHST software package.[21]

Volume renderings of the cell density obtained by phase nanotomography are shown in Figs. 3(a) and 3(b), as well as virtual slices through the volume in Fig. 3(c) (Multimedia view). Detailed morphological features are revealed thanks to the high sensitivity of multiple distance phase retrieval. To obtain the thickness map, we carried out a morphological segmentation of the cell, based on the values of the electronic density, obtaining binary masks of slices which were summed up along the normal to the surface of the substrate. The resulting thickness map in Fig. 4(a) is compared with the measurement on the same cell with AFM in Fig. 4(b). The comparison shows a very good agreement in both the general morphology and in the absolute thickness values (see also supplementary material, S2), with an average cell thickness of 0.26 μm and 0.23 μm, respectively, according to nanotomography and AFM. One can recognize the presence of some large and deep pores in the tomographic data. These pores result probably from the freeze-drying process leading to ice crystal formation or from the osmotic changes upon rinse using biological buffers. These pores are less or not visible in the AFM data because AFM only measures the

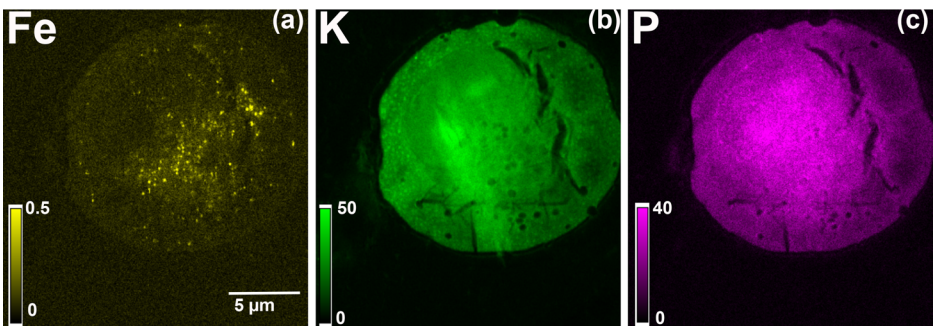

FIG. 2. X-ray fluorescence areal density maps (ng/mm^2) of (a) iron, (b) potassium, and (c) phosphorus.

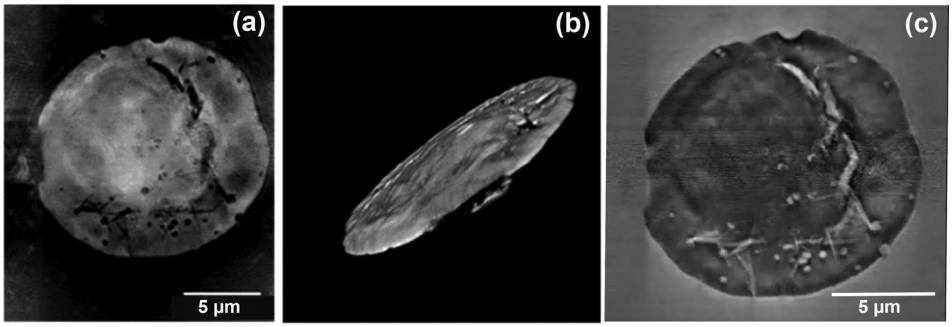

FIG. 3. Volume rendering of the cell density obtained by X-ray phase nanotomography in (a) front and (b) lateral perspectives and (c) slice through the macrophage cell obtained by X-ray phase nanotomography. Multimedia view: https://doi.org/10.1063/1.5008834.1

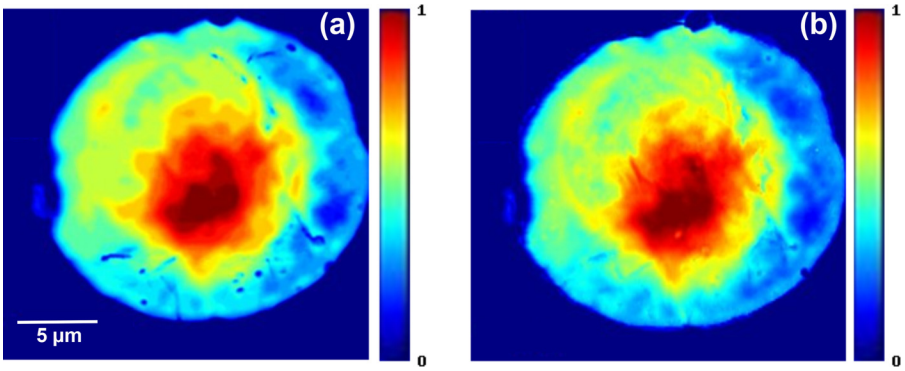

FIG. 4. Cell thickness map (μm) obtained by (a) holotomography and (b) AFM.

topology of the cell, whilst the 3D volume information in tomography can reveal the inhomogeneity below the surface as well. The thickness map is registered with respect to the P fluorescence data using the FLIRT software of the FSL tool.[22] After registration, the concentration map of a given element c_{el} is obtained by normalizing the areal density map D_{el} pixel by pixel with the thickness map T using the expression

$$c_{\mathrm{el}} = \frac{(D_{\mathrm{el}} - D_{\mathrm{el,bg}})}{A_{\mathrm{el}}} \frac{T}{T^2 + T_{\mathrm{min}}^2} \qquad (1)$$

with the atomic weight A_{el} and the minimum cell thickness T_{min}. The background of the areal density $D_{\mathrm{el,bg}}$ is determined as the average outside the cell where $T < T_{min}$. The last term in expression (1) is similar to a Wiener deconvolution and handles the singularity when $T \approx 0$. T_{min} is set to 100 nm, twice the pixel size in the phase nanotomography data. The concentration maps in molarity of iron, potassium, and phosphorus are shown in Fig. 5. From the comparison of Figs. 2 and 5, one can see that after the normalization, at the level of 100 nm spatial resolution, the potassium concentration is roughly uniform throughout the cell while phosphorus shows clearly a higher intranuclear concentration mainly related to nucleic acids (DNA and RNA). The average potassium concentration inside the cell is 0.84 M. While the potassium concentration depends on the cell type and the preparation procedure,[2] our value agrees well with the value of 0.6 M reported for human macrophage monocytes.[23] Similarly, our average phosphorus concentration is 1.46 M in reasonable agreement with the range of 0.6–0.7 M reported in the literature.[23] It should be noted that the measured concentrations are somewhat overestimated compared to the fully hydrated state as the freeze-drying necessarily leads to a volume reduction. The average iron concentration of 1.2 mM is very low, but the Fe concentration reaches values of up to 0.03 M in hotspots located outside the nucleus. These Fe hotspots can be assigned to the presence of ferritin, the main iron storage protein in cells and particularly macrophages.[24] The brightest hotspot of Fe in Fig. 2 contains per pixel about 1.3×10^5 atoms or 43 ferritin molecules assuming an average of 3000 Fe atoms per molecule.[25] The concentration values are averaged over the footprint of the beam and the sample thickness.[26]

In conclusion, we demonstrate the feasibility of a correlative "whole X-ray" approach to determine quantitatively the intracellular molar concentration of a single macrophage

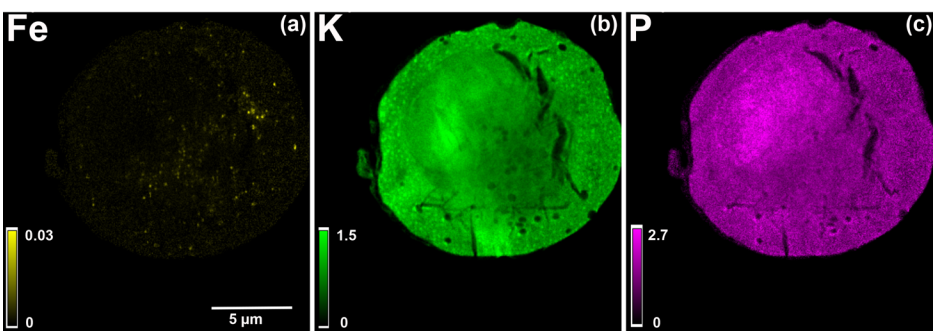

FIG. 5. Concentration maps [M] obtained by normalizing the fluorescence areal density maps with the thickness obtained by X-ray phase nanotomography. (a) Iron, (b) potassium, and (c) phosphorus.

cell at nanoscale spatial resolution by combining hard X-ray fluorescence and X-ray phase nanotomography measurements. This method employed the strengths of these techniques: the high elemental sensitivity and the improved 3D electron density contrast. The non-destructive method can reveal absolute concentration variations at the sub-cellular level, such as the organelles with a high precision. This proof of principle was performed on freeze-dried cells in order to compare with AFM measurements. However, more importantly, the potential of the method can be explored when the morphology information of the sample, especially in 3D, cannot be easily accessed, e.g., in frozen-hydrated cells. This work illustrates the power of the hard X-ray nanoprobe developed at beamline ID16A-NI, ESRF, with access to both structural and compositional information through correlative X-ray microscopy.

See supplementary material for further information, in particular, thickness profiles obtained by AFM and X-ray phase nanotomography.

C.G. gratefully acknowledges COST Action MP1207 "Enhanced X-ray Tomographic Reconstruction: Experiment, Modeling, and Algorithms" for financing Short Term Scientific Missions allowing permanence at ESRF and the COST Action MP1203 "Advanced X-ray spatial and temporal metrology" for networking support. This research was granted by the Sapienza University of Rome to PV and FB. The authors thank the ESRF for granting beamtime in the framework of the proposal LS-2362.

[1]S. Bohic, A. Simionovici, A. Snigirev, R. Ortega, G. Devès, D. Heymann, and C. G. Schroer, Appl. Phys. Lett. **78**, 3544 (2001).
[2]Q. Jin, T. Paunesku, B. Lai, S. C. Gleber, S. Chen, L. Finney, D. Vine, S. Vogt, G. Woloschak, and C. Jacobsen, J. Microsc. **265**, 81 (2017).
[3]C. Sanchez-Cano, I. Romero-Canelón, Y. Yang, I. J. Hands-Portman, S. Bohic, P. Cloetens, and P. J. Sadler, Chem. Eur. J. **23**, 2512 (2017).
[4]L. Vincze, K. Janssens, F. Adams, M. L. Rivers, and K. W. Jones, Spectrochim. Acta, Part B **50**, 127 (1995).
[5]B. Golosio, A. Simionovici, A. Somogyi, L. Lemelle, M. Chukalina, and A. Brunetti, J. Appl. Phys. **94**, 145 (2003).
[6]S. Lagomarsino, S. Iotti, G. Farruggia, A. Cedola, V. Trapani, M. Fratini, I. Bukreeva, A. Notargiacomo, L. Mastrototaro, C. Marraccini, A. Sorrentino, I. McNulty, S. Vogt, D. Legnini, S. Kim, A. Gianoncelli, J. A. M. Maier, and F. I. Wolf, Spectrochim. Acta, Part B **66**, 834 (2011).
[7]E. Malucelli, S. Iotti, A. Giannoncelli, M. Fratini, L. Merolle, A. Notargiacomo, C. Marrancini, A. Sargenti, C. Cappadone, G. Farruggia, I. Bukreeva, M. Lombardo, C. Trombini, J. A. Maier, and S. Lagomarsino, Anal. Chem. **86**, 5108 (2014).
[8]E. Kosior, S. S. H. Suhonen, R. Ortega, G. Devès, A. Carmona, F. Marchi, J. F. Guillet, and P. Cloetens, J. Struct. Biol. **177**, 239 (2012).
[9]M. D. de Jonge, B. Hornberger, C. Holzner, D. Legnini, D. Paterson, I. McNulty, C. Jacobsen, and S. Vogt, Phys. Rev. Lett. **100**, 163902 (2008).
[10]C. Holzner, M. Feser, S. Vogt, B. Hornberger, S. B. Baines, and C. Jacobsen, Nat. Phys. **6**, 883 (2010).
[11]D. J. Vine, D. Pelliccia, C. Holzner, S. B. Baines, A. Berry, I. McNulty, S. Vogt, A. G. Peele, and K. A. Nugent, Opt. Express **20**, 18287 (2012).
[12]J. Deng, D. J. Vine, S. Chen, Q. Jin, Y. S. G. Nashed, T. Peterka, S. Vogt, and C. Jacobsen, Sci. Rep. **7**, 445 (2017).
[13]F. Xu, L. Helfen, H. Suhonen, D. Elgrabli, S. Bayat, P. Reischig, T. Baumbach, and P. Cloetens, PLoS One **7**, e50124 (2012).
[14]M. D. de Jonge, C. Holzner, S. B. Baines, B. S. Twining, K. Ignatyev, J. Diaz, D. L. Howard, D. Legnini, A. Miceli, I. McNulty, C. Jacobsen, and S. Vogt, Proc. Natl. Acad. Sci. U. S. A. **107**, 15676 (2010).
[15]R. Paesano, T. Natalizi, F. Berlutti, and P. Valenti, Pathog. Global Health **106**, 200 (2012).
[16]P. Valenti, A. Catizone, A. Frioni, and F. Berlutti, Diet Exercise Cystic Fibrosis **30**, 259–270 (2014).
[17]G. Cairo, S. Recalcati, A. Mantovani, and M. Locati, Trends Immunol. **32**, 241 (2011).
[18]G. Casanova, F. Nolin, L. Wortham, D. Ploton, and V. Banchet, J. Michel, Micron **88**, 77–83 (2016).
[19]V. Sole, E. Papillon, M. Cotte, P. Walter, and J. Susini, Spectrochim. Acta, Part B **62**, 63 (2007).
[20]P. Cloetens, W. Ludwig, J. Baruchel, D. Van Dyck, J. Van Landuyt, J. P. Guigay, and M. Schlenker, Appl. Phys. Lett. **75**, 2912 (1999).
[21]A. Mirone, E. Brun, E. Gouillart, P. Tafforeau, and J. Kieffer, Nucl. Instrum. Methods Phys. Res., Sect. B **324**, 41 (2014).
[22]See http://fsl.fmrib.ox.ac.uk/fsl/flirt/ for more information about the program used for the thickness map registration (last accessed February 05, 2013).
[23]J. N. Skepper, I. Karydis, M. R. Garnett, L. Hegyi, S. J. Hardwick, A. Warley, M. J. Mitchinson, and N. R. B. Cary, J. Pathol. **188**, 100 (1999).
[24]E. Gammella, P. Buratti, G. Cairo, and S. Recalcati, Metallomics **6**, 1336 (2014).
[25]G. R. Bakker and R. F. Boyer, J. Biol. Chem. **261**, 13182 (1986).
[26]H. Koen, A. Janssens, C. Freddy, V. Adams, and A. Rindby, *Microscopic X-Ray Fluorescence Analysis* (Wiley, 1981), pp.170–178.